Formation and Aging of Secondary Organic Aerosol from Toluene: Changes in Chemical Composition, Volatility and Hygroscopicity

L. Hildebrandt Ruiz[1,2], A. L. Paciga[2*], K. Cerully[3#], A. Nenes[3], N. M. Donahue[2], S. N. Pandis[2,4]

[1] {The University of Texas at Austin, Austin, Texas, USA}

[2] {Carnegie Mellon University, Pittsburgh, Pennsylvania, USA}

[3] {Georgia Institute of Technology, Atlanta, Georgia, USA}

[4] {University of Patras, Patras, Greece}

[*] Now at Phillips66®, Bartlesville, OK

[#] Now at TSI, Inc., Shoreview, MN

Correspondence to: Lea Hildebrandt Ruiz (lhr@che.utexas.edu)

1 Abstract

Secondary organic aerosol (SOA) is transformed after its initial formation, but this chemical aging of SOA is poorly understood. Experiments were conducted in the Carnegie Mellon environmental chamber to form secondary organic aerosol (SOA) from the photo-oxidation of toluene and other small aromatic volatile organic compounds (VOCs) in the presence of NO_x under different oxidizing conditions. The effects of oxidizing condition on organic aerosol (OA) composition, mass yield, volatility and hygroscopicity were explored. Higher exposure to the hydroxyl radical resulted in different OA composition, average carbon oxidation state (OS_c) and mass yield. The OA oxidation state generally increased during photo-oxidation, and the final OA OS_c ranged from -0.29 to 0.16 in the performed experiments. The volatility of OA formed in these different experiments varied by as much as a factor of 30, demonstrating that the OA formed under different oxidizing conditions can have significantly different saturation concentration. There was no clear correlation between hygroscopicity and oxidation state for this relatively hygroscopic SOA.

15 1   Introduction

Secondary organic aerosol (SOA) is produced when gas-phase precursors are oxidized, forming lower volatility products that partition to the condensed phase. As SOA is estimated to account for approximately 70% of total aerosol organic carbon mass (Hallquist et al., 2009), the influence of SOA on aerosol composition and related properties is important and complex (Donahue et al., 2009; Kanakidou et al., 2005; Kroll and Seinfeld, 2008). Using measurements in urban, suburban, and remote sites, Zhang et al. (2007) showed that as aerosol ages in the atmosphere it reaches a highly oxidized state and no longer resembles either fresh primary or secondary aerosol.

Although it is clear that oxidation of gas-phase compounds and continued oxidation of particle-phase compounds play an important role in SOA production and transformation, the underlying chemistry and thermodynamics are poorly understood. Without the correct representation of SOA production and evolution mechanisms, modeling attempts often lead to underestimations of ambient mass loadings (Heald et al., 2005; Volkamer et al., 2006). The large uncertainty in SOA concentrations predicted by Chemical Transport Models (CTMs) demonstrates the need for experimental data on the multi-generation oxidation reactions or "aging" that lead to changes in

1 mass loadings and physicochemical properties of SOA. Several computational studies have

2 highlighted the importance of not only incorporating extended chemical mechanisms but obtaining

3 corresponding relationships between chemical aging and physiochemical properties of the SOA,

4 such as its volatility, in atmospherically relevant systems (Cappa and Wilson, 2012; Shrivastava

5 et al., 2013).

6 Considering the current state-of-the-science in aerosol analysis techniques, identifying the plethora

7 of SOA components and their individual volatilities is not possible. A unified framework to

8 evaluate complex systems in field or laboratory studies and to track changes in volatility as a

9 function of physicochemical processing is the 2D-Volatility Basis Set (2D-VBS). It uses

10 coordinates of volatility in terms of effective saturation concentration, C^*, and oxidation state of

11 carbon, OS_c (or the oxygen to carbon ratio, O:C) to provide a space suitable for the description of

12 the chemical transformations and phase partitioning of SOA (Donahue et al., 2012). Chemical

13 species are lumped by C^* and OS_c in discretized bins.

14 The relationship between organic aerosol (OA) hygroscopicity and extent of oxidation, indicated

15 by O:C, has been the focus of a number of laboratory and field studies (Alfarra et al., 2013; Chang

16 et al., 2010; Frosch et al., 2011; Jimenez et al., 2009; Lathem et al., 2013; Massoli et al., 2010).

17 While OA hygroscopicity often increases with O:C, some other studies have found weak or no

18 correlation between the two properties (Alfarra et al., 2013; Frosch et al., 2011; Lathem et al.,

19 2013; Massoli et al., 2010). It has been shown that OS_c is likely a better indicator of aerosol

20 oxidation than O:C as the latter can be affected by non-oxidative processes such as hydration and

21 dehydration while OS_c increases continually with oxidation (Canagaratna et al., 2015; Kroll et al.,

22 2009, 2011); thus, O:C may not be as well correlated with observed hygroscopicity.

23 The organic aerosol O:C has been proposed to be linked with its volatility in addition to its

24 hygroscopicity (Jimenez et al., 2009), and a few chamber studies have investigated the link among

25 all three properties (Poulain et al., 2010; Tritscher et al., 2011). The conventional view is that the

26 most volatile components should be the least hygroscopic; however, several studies have observed

27 the opposite behavior (Asa-Awuku et al., 2009; Cerully et al., 2014; Meyer et al., 2009; Poulain et

28 al., 2010). Tritscher et al. (2011) found that hygroscopicity and O:C remained constant with

29 decreased volatility for α-pinene SOA during aging by OH radicals.

1   We investigated the relationship between oxidation, volatility and hygroscopicity of SOA formed

2   from the photo-oxidation of toluene (methylbenzene) and other small aromatic volatile organic

3   compounds (VOCs) under a variety of oxidation conditions. Small aromatics are important

4   anthropogenic SOA precursors (Pandis et al., 1992; Vutukuru et al., 2006), and toluene serves as

5   a model system to study the formation of SOA from these compounds. A main objective of our

6   work is to connect the extent of oxidation and the changes in volatility of these experiments within

7   the 2D-VBS framework.

8

9   2   Materials and Methods

10   2.1   Environmental Chamber Experiments

11 Organic aerosol was formed from the photo-oxidation of toluene and other small aromatic VOCs

12 in the Carnegie Mellon Center for Atmospheric Particle Studies (CAPS) environmental chamber.

13 The basic sequence of the experiments was to fill the chamber with clean air, inject the VOC and

14 nitrous acid (HONO), and turn on the UV lights to start formation of OH (from the photolysis of

15 HONO), oxidation of the VOC and formation of secondary organic aerosol (SOA). The number

16 of UV lights used, the initial VOC concentrations, and the number of HONO injections was varied

17 between experiments in order to create different oxidizing environments, as summarized in Table

18 1. The amount of SOA formed, the SOA oxidation state, its volatility and its hygroscopicity were

19 then measured as explained in more detail below.

20 Nitrous acid was produced immediately before injection by drop-wise addition of 12 ml 0.1 M

21 sodium nitrite solution to 24 ml 0.05 M sulfuric acid solution. Ammonium sulfate ($(NH_4)_2SO_4$,

22 Sigma Aldrich, 99.99%)) seed particles were used in some experiments (Table 1) to provide

23 surface area onto which organics would condense as SOA. In the unseeded experiments, nucleation

24 of the organic vapors was observed. With the exception of Experiment 7 (Table 1), isotopically

25 labeled toluene was used (^{13}C-toluene, Cambridge Isotope Laboratories, 99%) as in a previous

26 study (Hildebrandt et al., 2011). All six ring carbons in the labeled toluene are ^{13}C-substituted,

27 leaving the methyl carbon unsubstituted. In two experiments (Expts. 6 and 8) other small aromatic

28 compounds were injected in addition to toluene as detailed in Table 1 in order to test whether these

29 VOCs behave similarly as toluene. Concentrations of the VOCs were monitored using a proton-

transfer reaction mass spectrometer (PTR-MS, Ionicon Analytik GmbH) when available. PTR-MS measurements were corrected for ion-source intensity and humidity as suggested by de Gouw et al. (2003). The sensitivity of the PTR-MS to the VOCs was measured before each experiment using a calibration gas mixture.

Figure 1 illustrates the experimental setup. Particle number and volume of the chamber aerosol were measured using a scanning mobility particle sizer (SMPS), comprised of a TSI model 3080 classifier and a TSI model 3772 condensation particle counter (CPC). Particle mass and chemical composition was measured using a high-resolution time-of-flight aerosol mass spectrometer (AMS) from Aerodyne, Inc. (DeCarlo et al., 2006). The AMS has two ion optical modes named by the shape of the ion flight paths: a single-reflection mode (V-mode) with a shorter flight path and hence higher sensitivity but lower resolution, and a double-reflection mode (W-mode) with longer flight path and hence higher resolution but lower sensitivity. In this study the AMS was operated according to the common protocol with the vaporizer temperature at 600°C, alternating between V and W modes to collect mass spectra, and collecting particle time-of-flight (pToF) measurements in V-mode.

Air from the chamber was split into two separate streams for analysis of OA concentrations and properties. In the first stream, OA volatility was probed using a thermodenuder (TD) system, similar to the system used in Lee et al. (2010). Aerosol was passed alternately through the TD, heated to a predefined temperature, or a bypass line and then to the SMPS and the AMS for measurements of the particle size distributions and chemical composition. Properties of thermally-treated OA were determined by comparing the residual aerosol after heating in the TD to the aerosol which was passed through the bypass line. The standard operating sample flowrate for the TD was 1 liter per minute (LPM), corresponding to a centerline residence time of ~15 s. In the TD followed by the AMS, the flow rate was also sometimes set to 0.6 LPM, corresponding to a centerline residence time of ~25 s, to evaluate the effects of a longer residence time on OA evaporation, though these data were not used for thermally-denuded CCN comparisons.

In the second stream, aerosol was again passed alternately through the TD or bypass line, then size-selected (approximately 100 to 140 nm) using a differential mobility analyzer (DMA, TSI model 3080) operated with a sheath to aerosol ratio of 10:1. Aerosol flow was then split to a CPC (TSI model 3010) and a cloud condensation nuclei counter (CCNc, Droplet Measurement

Technologies). The CCNc was operated in Scanning Flow CCN Analysis (SFCA) mode (Moore et al., 2010), allowing for fast measurements of CCN by scanning the flow rate through the CCNc column, which measured the OA hygroscopicity. The thermodenuder positioned before the CCNc operated under the same temperature conditions as the AMS-TD and had a sample flowrate of 1 LPM, which allows for analysis of volatility and hygroscopicity of the complete OA and the thermally denuded OA. Dilution air of 1.1 LPM was introduced after the DMA before splitting to the CCNc and CPC. Flow to the CCNc was held constant at 1.1 LPM using a laminar flow element, while flow in the CCNc was linearly ramped between 0.1 and 0.9 L min^{-1} over 60 s. The top to bottom column temperature difference was 6°C for all experiments.

2.2   AMS Data Analysis

The AMS data were processed in Igor Pro 6.12 (Wavemetrics, Inc.) using the standard AMS data analysis toolkits "Squirrel" version 1.51C for unit mass resolution (UMR) analysis and "Pika" version 1.10C for high resolution (HR) analysis. HR analysis was performed using the W-mode data since highest resolution is preferred to distinguish between isotopically labeled and unlabeled ions. The lists of ions integrated in the HR analysis is similar to the list used previously (Hildebrandt et al., 2011). Ion masses were fitted up to an *m/z* ratio of 105; above this the signal was too noisy and/or the mass spectra were too crowded for reliable identification of ion atomic composition. According to the UMR analysis more than 95% of the organic signal was below *m/z* 105, and the total organic mass was corrected based on this fraction calculated for each experiment (Table S1).

2.2.1   Modification of Standard Fragmentation Table

Several adjustments were made to the standard fragmentation table (Allan et al., 2004) for the analysis of HR and UMR data as explained in detail in the supplementary material; only the most important adjustments are summarized here. First, the fragmentation table was adjusted to account for hydrogen atoms (*m/z* = 1) formed in the fragmentation of H_2O (Canagaratna et al., 2015). Second, the amount of H_2O^+ attributed to organics was chosen so that the mass of water does not correlate with the mass of organics (R < 0.01) as expected for these low relative humidity

experiments. The ratios of organic H_2O^+ to $(^{13}CO_2^+ + CO_2^+)$ are provided in Table 2 and ranged from 0.3 to 2.4, higher than the ratio of 0.225 in the default fragmentation table but consistent with recent calibration experiments (Canagaratna et al., 2015). Third, ions assigned to the nitrate family in the HR analysis (NO^+, NO_2^+) were added to the total organic aerosol mass in the HR batch table because they appear to be due to organic nitrates: The ratio of NO^+ to NO_2^+ measured in these experiments (Table 2) is around 8, much higher than the ratio of 2.4 measured in calibration experiments using ammonium nitrate. Furthermore, no inorganic nitrate was added in these experiments. Nitric acid is expected to form in the gas phase but does not appear to partition appreciably to the particle phase, consistent with its high vapor pressure (Fry et al., 2009). Nitrate fragments were not included in the calculation of O:C and H:C since elemental analysis examines the oxidation state of the carbon atoms.

2.2.2 Quantification of Organic Aerosol Production

Data were corrected for changes in the instrument air beam (AB) over the course of an experiment. The ionization efficiency (IE) for each experiment was adjusted based on the ratio of the AB during the experiment to the AB during the ionization efficiency calibration conducted before this set of experiments was started (calibration IE/AB = 4.65×10^{-13}). Additional details on quantification of AMS data are provided in the supplementary material. The AMS collection efficiency (CE) for these data was estimated by matching AMS mass distributions and SMPS volume distributions using the OA density (ρ_{org}) and AMS CE as fitting parameters, with the algorithm developed by Kostenidou et al. (2007) .

The amount of organic aerosol formed was quantified as the fractional aerosol mass yield (mass of OA formed divided by mass of toluene reacted). The mass of OA formed was corrected for the depositional loss of particles onto the chamber walls and for the condensational loss of organic vapors to wall-deposited particles. The assumption was made that condensation of organic vapors is not slowed by mass-transfer resistances, and that the wall-deposited particles are in equilibrium with the organic vapors in suspension. Therefore, the total (corrected) concentration of OA can be calculated by multiplying the OA/seed ratio by the initial seed concentration, as discussed in more detail in Hildebrandt et al. (2009). This correction does not account for condensation of organic vapors onto the "clean" Teflon walls. While these losses have been shown to occur (e.g. Matsunaga

1 and Ziemann, 2010), quantification of their magnitude is an area of active research and remains

2 challenging.

3 In all of the experiments described here, the condensation sink after particle formation was

4 approximately 1 min^{-1}, while the initial condensation sink to ammonium sulfate seeds in seeded

5 experiments ranged between 0.6 and 1 min^{-1}. The timescale for sulfuric acid vapor wall loss in

6 the Carnegie Mellon chamber is approximately 0.1 min^{-1}, as determined by chemical ionization

7 mass spectrometer measurement of sulfuric acid loss (V. Hofbauer, personal

8 communication). Thus, in all of the seeded experiments, condensing vapors encountered the seeds

9 approximately 10 times before encountering the walls, while in nucleation experiments the

10 suspended aerosol population quickly grew to a size where this was also true. Thus, while wall

11 losses of semi-volatile vapors are a source of uncertainty, we have attempted to ensure that vapor-

12 particle interactions at least dominate over vapor-wall interactions. It is therefore reasonable to

13 expect that observed differences between experiments are not driven by interactions with the walls

14 but instead by chemical processing of the organic aerosol.

15

2.3   Analysis of Organic Aerosol Volatility

2.3.1   Data Preparation

18 Volatility data were collected for each experiment after the SOA had formed. During some

19 experiments, measurements were also made during the irradiation period (with the UV lights on)

20 to examine the volatility changes during photo-oxidation. TD data are analyzed in terms of Volume

21 Fraction Remaining (VFR) or Mass Fraction Remaining (MFR). Using the total organic mass

22 concentration from the AMS, the MFR was calculated by dividing the mass concentration of the

23 denuded OA by the mass concentration of the OA that had passed through the bypass. These data

24 are presented in the form of a thermogram, which shows the MFR as a function of temperature in

25 the TD.

26 Particle concentrations decline in the smog chamber after SOA formation chemistry ceases due to

27 losses to the chamber walls. This can lead to biases in the estimated MFR when bypass

28 concentrations before or after the TD sampling period are used. A more accurate MFR was

29 obtained by interpolation of the bypass OA concentrations corresponding to the TD sampling

times. Each experiment was analyzed individually for a best fit, usually resulting in an exponential decay function. Graphs of the interpolated bypass data are shown in Fig S2.

Particle losses in the TD were also taken into account. These losses occur due to diffusion (primarily of small particles), sedimentation (primarily of large particles), and thermophoresis; the losses are therefore a function of sample flow rate, temperature, and particle size (Burtscher et al., 2001). To estimate the losses within the TD setup, size dependent loss functions were developed using NaCl particles under various TD temperatures and sample flow rates (Lee and Pandis, 2010). The number losses for each TD temperature – residence time combination are calculated by determining the losses over the size distribution measured by the SMPS. The number losses for each size bin are then converted to a volume-based correction using the particle diameter of each bin. This correction factor is applied to the calculated MFR values. The organic MFR was calculated from AMS bypass and thermodenuder mass concentrations averaged over 6-9 minutes for a given TD temperature and residence time. It is assumed that there are no significant changes to composition and volatility over these averaging periods.

2.3.2   Evaporation model

Due to the non-equilibrium conditions in the TD, a dynamic mass transfer model developed by Riipinen et al. (2010) was used to estimate the relative volatility of the OA formed in the experiments outlined in Table 1. Briefly, aerosol evaporation is simulated using experimental inputs including TD temperature, residence time, particle mode diameter, mass concentration, and OA density. This method utilizes the volatility basis set approach (Donahue et al., 2006) to account for the component complexity in the SOA formed. Assuming the particles are in equilibrium with the vapor phase as they enter the TD, the effective saturation concentration is estimated from a least-squares fit to the experimental thermograms. An important caveat to this approach is that physical properties including mass accommodation coefficient and enthalpy of vaporization, which are usually unknown, can substantially affect the volatility estimated (Lee et al., 2010) . The primary goal of these experiments was to observe changes in OA volatility with different levels of oxidation. Thus, relative volatility changes were calculated as described below, thus reducing uncertainties arising from the choice of accommodation coefficient and enthalpy of vaporization.

The volatility of SOA formed in each experiment was determined assuming a fixed volatility distribution shape using four saturation concentrations, 1, 10, 100, and 1000 $\mu g\ m^{-3}$. During the

1   analysis the saturation concentrations are multiplied by a shifting factor, s. This practically shifts

2   the volatility distribution to lower or higher values assuming that the shape of the distribution does

3   not change. Differences in shifting factors can then be interpreted as differences in the saturation

4   vapor pressure of the OA formed in these experiments: for example, OA with shifting factor 10 is

5   ten times more volatile than the OA with shifting factor 1. The volatility distribution used is the

6   fresh toluene SOA distribution estimated by Hildebrandt et al. (2009) for their high NO_x

7   experiments: 0.025 for $C^* = 1$, 0.51 for $C^* = 10$, 0.38 for $C^* = 100$, and 0.085 for $C^* = 1000$ μg

8   m^{-3}. The shifting factor is estimated for each of the experiments presented here by using the mass

9   transfer model and least squares fitting to the MFRs. In the last step relative shifting factors are

10   calculated by normalizing them by the shifting factor of the OA formed in Expt. 7, in which SOA

11   had the lowest OS_c. In this way, the relative volatility reduction ($1/s$) for each experiment is

12   estimated while accounting for the experiment specifics including residence time, TD temperature,

13   mass concentration, and particle size. Fixed values are used for the enthalpy of vaporization (80

14   kJ mol^{-1}) and the mass accommodation coefficient (1.0). The sensitivity of results to these choices

15   is discussed in Section 3.2.

16

2.4   Analysis of CCN Activity

2.4.1   CCNc calibration

19   The CCNc instrument calibration is used to determine the relationship between instantaneous

20   instrument flow rate and supersaturation as described in Moore et al. (2010). Ammonium sulfate

21   solution is atomized, dried using a silica gel diffusion dryer, charge-neutralized using Po-210, and

22   classified by a DMA. The flow is then introduced into both a CPC and a CCNc. The activation

23   ratio, or the ratio of CCN to total particles, is then plotted against the instantaneous flow rate to

24   yield data that are fit to a sigmoidal activation ratio function. The critical flow rate, Q^*, is

25   determined, corresponding to where half of the total particles are activated and to a level of

26   supersaturation, s^*, equal to the critical supersaturation of the classified aerosol (Section 2.4.2).

27   The Q^* and s^* are determined for a range of aerosol sizes, yielding, for the flow rate range (0.1-

28   0.9 L min^{-1}) and temperature gradient ($\Delta T=6°C$) in the CCNc column, supersaturations ranging

29   from approximately 0.1 to 0.5%.

30

2.4.2 Calculating aerosol hygroscopicity of size-selected aerosol

Using the method outlined in Section 2.4.1, s^* was determined for each flow rate upscan and downscan. All CCNc data subject to poor counting statistics (where the maximum CCN concentrations were lower than approximately 15 to 20 counts cm^{-3}) were excluded from analysis (Moore et al., 2010). The characteristic hygroscopicity parameter, κ (Petters and Kreidenweis, 2007), of the monodisperse CCN is then determined by

$$\kappa = \frac{4A^3}{27d_p^3 s^{*2}} \tag{1}$$

where $A=(4M_w\sigma_w)/(RT\rho_w)$; M_w, σ_w, and ρ_w are the molar mass, surface tension, and density of water, respectively. R is the universal gas constant, T is CCNc mid-column temperature, and d_p is the dry particle diameter selected by the DMA prior to the CCNc.

3   Results and Discussion

3.1   Organic aerosol concentration, composition and mass yield

Figure 2 shows the time series of OA concentrations and oxidation state for an unseeded experiment (2, top panel) and a seeded experiment (9, bottom panel). The time series of toluene concentrations are also shown for Expt. 9; these data were not available for Expt. 2. There were two photo-oxidation periods ("lights on") during each experiment, and HONO was injected every time before lights were turned on. During experiment 2, the OA was alternatively passed through the bypass and the TD throughout the experiment (only the bypass data are shown in Fig 2). The TD was held at the same temperature during the photo-oxidation periods to observe changes in volatility during this period, and the temperature in the TD was varied during the dark period to obtain a thermogram. During experiment 9, the OA was passed only through the bypass during photo-oxidation, and it was alternated between bypass and TD (at different temperatures) during the dark period. The OA concentrations increased during the oxidation periods (lights on) as toluene was oxidized to form SOA. Toluene concentrations decreased by approximately 50% during the first photo-oxidation period in Expt. 9 and decreased an additional 20% during the second photo-oxidation period. Thus, gas-phase toluene is always present in the system and fresh

1 toluene SOA is expected to form at the same time as the previously formed toluene SOA is aged

2 photo-chemically.

3 A moderate increase in the OA oxidation state was observed during the "lights on" period in both

4 experiments. Two competing effects can influence the OA oxidation state: First, according to

5 partitioning theory, species of increasingly higher volatility will partition to the particle phase as

6 the OA loading in the system increases. If oxidation state is anti-correlated with volatility this

7 effect would decrease oxidation state when OA concentration increases. Second, the existing OA

8 can be oxidized further (aged), increasing the OA oxidation state as long as the molecules

9 composing the OA do not fragment. The OA oxidation state of the OA formed increased for several

10 hours in the experiments shown in Figure 2 and all other experiments conducted as part of this

11 work, suggesting that the aging effect dominated.

12 In an attempt to produce highly oxidized OA, photo-oxidation of the OA was continued for over

13 24 hours during experiments 3 and 5. Figure 3 shows the time series of oxidation state and

14 elemental ratios (O:C and H:C) for Expt. 3. As before, HONO was injected before every irradiation

15 period. The OA oxidation state increased during the first few hours of irradiation but significantly

16 decreased after longer irradiation. Plausible explanations for this decrease in oxidation state (which

17 was also observed after long irradiation in experiment 5) include the condensation of less oxidized

18 vapors, photolysis of OA components and their fragmentation after continued oxidation with OH.

19 Fragmented products may have a high oxidation state but high volatility (due to their smaller size)

20 and evaporate from the OA, decreasing the OA average oxidation state. Photolysis of organic

21 compounds is expected to occur throughout the experiment (e.g. Surratt et al., 2006), but as long

22 as OH reactions dominate the oxidation state of the bulk OA increases. Future experiments should

23 aim to isolate OH from photolysis reactions by, for example, using a dark OH source. This would

24 help to constrain these effects and eventually represent them in chemical transport models.

25 Table 2 provides a summary of the OA composition for all experiments investigated here. The

26 observed oxidation state of the OA formed ranged from -0.29 to 0.16. At least 10% of the OA

27 mass was due to the sum of NO^+ and NO_2^+ ions. The observed ratio of NO^+ to NO_2^+ (Table 2) was

28 between 7.0 and 8.6, much higher than the ratio of 2.4 measured in calibration experiments using

29 ammonium nitrate, suggesting that the NO^+ and NO_2^+ ions originate from organic nitrogen (ON)

30 compounds. Estimating that the ON compounds have an average molecular weight of about 200 g

mol^{-1}, approximately half of the OA is due to ON. Thus, organic nitrogen compounds are a major
constituent in the OA formed in these high-NO$_x$ photo-oxidation experiments.

In experiments 6 and 8, other small aromatic VOCs were injected in addition to toluene. The OA
formed in these experiments did not stand out in terms of its composition, volatility (Section 3.3)
or hygroscopicity (Section 3.4). This suggests that other small aromatic VOCs behave similarly as
toluene and that toluene can be used as a model system to study small aromatic VOCs.

3.2   High and low oxidation experiments – a case study

This section compares two seeded experiments (number 7 and 9, Table 1) and two unseeded
experiments (number 2 and 4). The aim in the design of these experiments was to create different
photochemical conditions. Therefore, fewer HONO injections were performed, more toluene was
injected, fewer lights were used (resulting in lower UV intensity), and the irradiation period was
shorter in Expt. 7 compared to Expt. 9 (10 minutes and 3 hours, respectively). The decay of toluene,
monitored by the PTR-MS, was used to estimate the OH exposure of the OA during irradiation.
Total OH exposure during Expt. 7 was 7-8 times lower than during Expt. 9. Figure 4 shows the
OA mass yields for experiments 7 and 9 as a function of the corrected OA concentration in the
system; only the first irradiation period was used for Expt. 9 as uncertainties due to wall losses
increase over the course of an experiment. The OA yields are higher for Expt. 9, which exhibited
higher OH exposure. Considering only the first irradiation period, OH exposure in Expt. 9 was
five times higher than in Expt. 9. The OA formed in Expt. 9 also exhibited significantly higher
oxidation state (~0, Table 2) than the OA formed in Expt. 7 (~-0.3), and its volatility was
approximately a factor of seven lower than the volatility of the OA formed in Expt. 7 (Table 2).

Previous work has suggested that higher OH exposures help to reduce wall losses (Kroll et al.,
2007); therefore, different oxidizing conditions could result in different wall-loss rates of semi
volatile vapors. As mentioned in section 2.2.2 above the changes observed in these experiments
seem to be driven by chemical processes, not by the interactions with chamber walls. Thus, the
higher oxidation state and lower volatility observed during Expt. 9 were likely a result of higher
OH exposure.

1   The OA mass yields shown in Fig 4 are lower than high NO_x OA mass yield measured in our

2   previous study (Hildebrandt et al., 2009), likely due to different initial and oxidizing conditions.

3   In the previous study the source of OH and NO_x was HOOH and NO, and all NO converted to

4   NO_2 within a few minutes of the start of photo-oxidation. In the present study the source of OH

5   and NO_x was HONO, and both NO and NO_2 were present throughout the experiments. Gas-phase

6   chemistry is primarily affected by the level of NO, not total NO_x, and lower OA mass yields are

7   expected under high NO, high NO_x conditions (present study) compared to high NOx low NO

8   conditions (Hildebrandt et al., 2009).

9   Differences in the OA composition are also apparent when comparing the total OA to the denuded

10   OA from these two experiments. Figure 5 (right panel) shows the difference in oxidation state of

11   the denuded and the total OA at the different TD temperatures for Expt. 7 and 9. For the less

12   oxidized, more volatile OA formed in Expt. 7, the oxidation state of the denuded OA is higher than

13   the oxidation state of the total OA, as expected when volatility correlates with oxidation state. The

14   difference is larger at the higher TD temperatures when a larger fraction of the total OA has

15   evaporated. However, for the more oxidized, less volatile OA formed in Expt. 9, the denuded OA

16   has essentially the same oxidation state as the total OA at all TD temperatures. This is consistent

17   with the OA being composed of molecules that have a similar oxidation state but different chain

18   length, resulting in different volatilities. A similar observation was made when sampling highly

19   oxygenated OA during ambient measurements in Finokalia, Greece, where the fraction of OA due

20   to fragments of *m/z* 44 was not significantly different for denuded and total OA (Hildebrandt et

21   al., 2010).

22   A similar comparison can be made for two non-seeded experiments (number 2 and 4), which

23   resulted in OA of different oxidation state and volatility (Table 2). Data from the PTR-MS were

24   not available for this experiment, hence, OH exposure could not be estimated and OA mass yields

25   could not be calculated, but it is likely that higher OH concentrations as well as lower OA

26   concentrations in Expt. 2 resulted in the more oxidized, less volatile OA. The OA formed in Expt.

27   4 had similar oxidation state as the OA formed in Expt. 9 mentioned above (~ 0). The OA formed

28   in Expt. 2 had the highest oxidation state of all OA analyzed here (~ 0.16), and its volatility was

29   about a factor of seven lower than the volatility of the OA formed in Expt. 4. The left panel of Fig

30   5 shows the difference in oxidation state (denuded vs. total) as a function of TD temperature for

31   Expts. 2 and 4. The OA formed in Expt. 4 exhibits similar behavior as the OA formed in Expt. 9,

with very little difference between the oxidation state of denuded and total OA. The OA in Expt. 2 shows a higher oxidation state for denuded OA than for non-denuded OA. Thus, it appears that for OA of lower and higher bulk oxidation state, the oxidation state anti-correlates with volatility, shown here as a higher oxidation state of the denuded OA. For OA of intermediate oxidation state (around zero), the volatility of the OA does not correlate significantly with bulk oxidation state. The volatility and oxidation state of OA formed in all experiments is analyzed further below.

3.3 Volatility

Figure 6 shows mass concentration time series measured during Experiment 7 including both the bypass and TD measurements. This experiment produced the least oxidized and most volatile SOA and serves as the baseline for comparison of OA volatility in the other experiments. HONO was injected into the chamber and, at t = 0, the UV lights in the chamber (30% of them) were turned on. The hydroxyl radical formed during the HONO photolysis began to react with toluene and the organic mass concentration increased due to the formation of SOA. The lights remained on for approximately 15 minutes and at that point the HONO photolysis was stopped by turning off the UV lights. The AMS then alternated between the bypass line and thermodenuder (operating at different temperatures and residence times) to obtain the thermogram shown in Fig 7. Half of the organic aerosol mass evaporated at 70°C (T_{50} temperature). For this and all other experiments, the MFR was nearly the same after 15 and 25 seconds residence time in the thermodenuder.

The 15 and 25 s residence time datasets were independently modeled, resulting in two estimates of volatility reduction for each experiment. These were quite similar (Table 2) for all cases suggesting that these measurements are consistent with the choice of a unity accommodation coefficient. The estimated relative volatility reductions relative to Experiment 7 for all experiments are presented in Table 2, and the experiment-specific model inputs (OA loading, particle mode diameter, and OA density) are presented in Table S2. Volatility was lower in other experiments by as much as a factor of 30, demonstrating that the OA formed under different oxidation conditions can have significantly different vapor pressure. A comparison of the modeled versus the measured MFRs is shown in Figure S3.

Sensitivity runs were performed in order to examine the effects of the accommodation coefficient and enthalpy of vaporization parameters. In summary, the analysis revealed that changing the mass

1 accommodation coefficients between 0.01, 0.1 and 1 for Expts. 7 and 9, which exhibited quite

2 different experimental conditions, changes neither the relative volatility reduction nor the

3 goodness of fit (represented by the sum of squared residuals, SSR) by more than 15%. In addition,

4 better least squares fits are obtained for enthalpy of vaporization of 80 kJ mol^{-1} (average SSR for

5 all nine experiments, SSR$_{avg}$ = 0.04) than for enthalpy of vaporizations of 20 kJ mol^{-1} or 120 kJ

6 mol^{-1} (SSR$_{avg}$ = 0.11 and 0.09, respectively). Changing the enthalpy of vaporization does not

7 change the trends in volatility reduction between experiments. More detailed results of the

8 sensitivity study are presented in the supplementary material.

9

3.3.1   Dependence of Volatility on Oxidation State

11 Differences in volatility of the toluene SOA in these experiments can be compared to its carbon

12 oxidation state (Fig. 8). The change in volatility is expressed as the logarithm of the volatility

13 reduction. This is consistent with the assumption of a constant volatility distribution shape shifting.

14 Each data point represents a single experiment in terms of volatility reduction or the change in log

15 C^* and the corresponding OS$_c$. In general, the more oxidized organic aerosol is less volatile. This

16 is consistent with functionalization reactions decreasing the volatility of the OA as it is oxidized.

17 Using a least squares fit, a straight line is fit to the dataset giving a relation of (OS$_c$) = 0.284

18 ($\Delta\log_{10} C^*$) - 0.245. This suggests that an increase of the oxidation state by approximately 0.3

19 units corresponds to a reduction of the average volatility by an order of magnitude for the toluene

20 SOA system examined here. However, as discussed in section 3.2, the volatility of individual

21 species composing the OA is not always correlated to their oxidation state.

22

3.4   Hygroscopicity

24 CCNc-derived organic hygroscopicity, κ_{org}, expressed as the average hygroscopicity of all

25 measured sizes, versus the bulk O:C ratio and OS$_c$ is shown in Fig. 9 for each experiment where

26 CCNc data were available. Throughout all experiments, κ_{org} ranges from 0.10 to 0.25 while bulk

27 O:C ranges from approximately 0.85 to 1.05. For each experiment, after the initial period of photo-

28 oxidation, κ_{org} remains fairly constant, as does O:C. There is no clear correlation between κ_{org} and

29 O:C (Fig 9 top, left) or between κ_{org} and OS$_c$ (Fig. 9 top, right) across all experimental conditions.

This is counter to the conventional view that oxidative aging of aerosol generally increases its hygroscopicity (Jimenez et al., 2009).

When investigating κ_{org} for Expts. 4 and 6 where both non-denuded and thermally-denuded measurements were collected, it appears that thermally-denuded aerosol (combined measurements from 60, 80, and 100°C) may show a slight decrease in κ_{org} with increased O:C (and OS$_c$) (Fig. 9 bottom). While the change in κ_{org} as well as O:C and OS$_c$ cannot be concluded with confidence due to the relatively large variation in κ_{org}, it is possible that this relationship between hygroscopicity and oxidation suggests that there may be another process, aside from bulk oxidation changes, causing changes in the measured hygroscopicity. Sareen et al. (2013) showed that gas-phase compounds such as methylglyoxal can act as surfactants, which depress surface tension and enhance CCN-activity (and hygroscopicity). As methylglyoxal as well as other gas-phase surface-active compounds such as benzaldehyde and glyoxal are known products of toluene oxidation by OH (Baltaretu et al., 2009), it is likely that gas-phase surfactants are present in these experiments. If surfactant films are present on the non-denuded aerosol, enhancing their hygroscopicity, then desorption of the surfactants later upon heating may increase surface tension and depress apparent hygroscopicity. A monolayer of surfactant adsorbed from the gas phase would induce a negligible impact on bulk O:C or OS$_c$. Thus, the volatility of OA would not necessarily correlate with its oxidation state if surfactants are present. Another potential explanation for the lack of a clear correlation between κ_{org} and OS$_c$ is that the OA composition is dominated by compounds with similar OS$_c$ but different size (e.g. oligomers), as the size of molecules affects their solubility and therefore their hygroscopicity.

4   Conclusions

Photochemical aging clearly influences anthropogenic SOA, and the general trend toward increased SOA mass and reduced volatility is consistent with progressive oxidation driving organic aerosol toward the highly oxidized, low-volatility endpoint observed around the world. There is a strong relationship between exposure to OH and physicochemical properties for SOA formed from the oxidation of toluene and other small aromatic VOCs. Organic nitrogen compounds are a major constituent in the SOA formed. An experiment with higher OH exposure showed higher SOA mass yields, more oxidized SOA, and reduced SOA volatility but only modest differences in

hygroscopicity. Volatility varied by a factor of 30 for different OH exposure, and a ten-fold decrease in volatility was associated with a 0.3 increase in carbon oxidation state. The SOA was relatively hygroscopic for organic material, with $0.1 < \kappa < 0.2$ and if anything a slightly negative relationship between kappa and oxidation state was observed, suggesting a possible role for surfactants or oligomeric compounds. The relationship between hygroscopicity, oxidation state and volatility may be modulated by gas-phase compounds.

While individual experiments with different OH exposure showed clear aging effects as different oxidation states and OA volatility, these effects were not evident within every single experiment. This suggests that a complex interplay exists between gas-phase processes, including oxidation reactions that both functionalize and fragment condensable organic species as well as photolysis of some species. The composition, hygroscopicity and volatility of organic aerosol do not always follow a prescribed relationship, highlighting the need for future laboratory experiments and ambient measurements which evaluate all of these properties.

Acknowledgements

References

Alfarra, M. R., Good, N., Wyche, K. P., Hamilton, J. F., Monks, P. S., Lewis, A. C. and McFiggans, G.: Water uptake is independent of the inferred composition of secondary aerosols derived from multiple biogenic VOCs, Atmos. Chem. Phys., 13, 11769–11789, doi:10.5194/acp-13-11769-2013, 2013.

1   Allan, J. D., Delia, A. E., Coe, H., Bower, K. N., Alfarra, M. R., Jimenez, J. L., Middlebrook, A.

2   M., Drewnick, F., Onasch, T. B., Canagaratna, M. R., Jayne, J. T. and Worsnop, D. R.: A

3   generalised method for the extraction of chemically resolved mass spectra from Aerodyne

4   aerosol mass spectrometer data, J. Aerosol Sci., 35(7), 909–922,

5   doi:10.1016/j.jaerosci.2004.02.007, 2004.

6   Asa-Awuku, A., Engelhart, G. J., Lee, B. H., Pandis, S. N. and Nenes, A.: Relating CCN

7   activity, volatility, and droplet growth kinetics of beta-caryophyllene secondary organic aerosol,

8   Atmos. Chem. Phys., 9, 795–812, doi:10.5194/acp-9-795-2009, 2009.

9   Baltaretu, C. O., Lichtman, E. I., Hadler, A. B. and Elrod, M. J.: Primary atmospheric oxidation

10   mechanism for toluene., J. Phys. Chem. A, 113(1), 221–30, doi:10.1021/jp806841t, 2009.

11   Burtscher, H., Baltensperger, U., Bukowiecki, N., Cohn, P., Huglin, C., Mohr, M., Matter, U.,

12   Nyeki, S., Schmatloch, V., Streit, N. and Weingartner, E.: Separation of volatile and non-volatile

13   aerosol fractions by thermodesorption: Instrumental development and applications, J. Aerosol

14   Sci., 32, 427–442, doi:10.1016/S0021-8502(00)00089-6, 2001.

15   Canagaratna, M. R., Jimenez, J.-L., Kroll, J. H., Chen, Q., Kessler, S. H., Massoli, P.,

16   Hildebrandt Ruiz, L., Fortner, E., Williams, L., Wilson, K., Surratt, J. D., Donahue, N. M.,

17   Jayne, J. T. and Worsnop, D. R.: Elemental Ratio Measurements of Organic Compounds using

18   Aerosol Mass Spectrometry: Characterization, Improved Calibration, and Implications, Atmos.

19   Chem. Phys., 15, 253–272, doi:10.5194/acp-15-253-2015, 2015.

20   Cappa, C. D. and Wilson, K. R.: Multi-generation gas-phase oxidation, equilibrium partitioning,

21   and the formation and evolution of secondary organic aerosol, Atmos. Chem. Phys., 12, 9505–

22   9528, doi:10.5194/acp-12-9505-2012, 2012.

23   Cerully, K. M., Bougiatioti, A., Hite Jr, J. R., Guo, H., Xu, L., Ng, N. L., Weber, R. and Nenes,

24   A.: On the link between hygroscopicity, volatility, and oxidation state of ambient and water-

25   soluble aerosol in the Southeastern United States, Atmos. Chem. Phys. Discuss., 14, 30835–

26   30877, 2014.

1 Chang, R. Y.-W., Slowik, J. G., Shantz, N. C., Vlasenko, a., Liggio, J., Sjostedt, S. J., Leaitch,

2 W. R. and Abbatt, J. P. D.: The hygroscopicity parameter (κ) of ambient organic aerosol at a

3 field site subject to biogenic and anthropogenic influences: relationship to degree of aerosol

4 oxidation, Atmos. Chem. Phys., 10, 5047–5064, doi:10.5194/acp-10-5047-2010, 2010.

5 DeCarlo, P. F., Kimmel, J. R., Trimborn, A. M., Northway, M. J., Jayne, J. T., Aiken, A. C.,

6 Gonin, M., Fuhrer, K., Horvath, T., Docherty, K. S., Worsnop, D. R. and Jimenez, J. L.: Field-

7 Deployable, High-Resolution, Time-of-Flight Aerosol Mass Spectrometer, Anal. Chem., 78,

8 8281–8289, 2006.

9 Donahue, N. M., Kroll, J. H., Pandis, S. N. and Robinson, a. L.: A two-dimensional volatility

10 basis set – Part 2: Diagnostics of organic-aerosol evolution, Atmos. Chem. Phys., 12, 615–634,

11 doi:10.5194/acp-12-615-2012, 2012.

12 Donahue, N. M., Robinson, A. L. and Pandis, S. N.: Atmospheric organic particulate matter:

13 From smoke to secondary organic aerosol, Atmos. Environ., 43, 94–106, 2009.

14 Donahue, N. M., Robinson, A. L., Stanier, C. O. and Pandis, S. N.: Coupled Partitioning,

15 Dilution, and Chemical Aging of Semivolatile Organics, Environ. Sci. Technol., 40, 2635–2643,

16 doi:10.1021/es052297c, 2006.

17 Frosch, M., Bilde, M., DeCarlo, P. F., Juranyi, Z., Tritscher, T., Dommen, J., Donahue, N. M.,

18 Gysel, M., Weingartner, E. and Baltensperger, U.: Relating cloud condensation nuclei activity

19 and oxidation level of α-pinene secondary organic aerosols, J. Geophys. Res., 116(D2212),

20 doi:10.1029/2011JD01640, 2011.

21 Fry, J. L., Kiendler-Scharr, A., Rollins, A. W., Wooldridge, P. J., Brown, S. S., Fuchs, H., Dube,

22 W., Mensah, A., dal Maso, M., Tillmann, R., Dorn, H. P., Brauers, T. and Cohen, R. C.: Organic

23 nitrate and secondary organic aerosol yield from NO3 oxidation of beta-pinene evaluated using a

24 gas-phase kinetics/aerosol partitioning model, Atmos. Chem. Phys., 9, 1431–1449,

25 doi:10.5194/acp-9-1431-2009, 2009.

De Gouw, J. A., Goldan, P. D., Warneke, C., Kuster, W. C., Roberts, J. M., Marchewka, M., Bertman, S. B., Pszenny, A. A. P. and Keene, W. C.: Validation of proton transfer reaction-mass spectrometry (PTR-MS) measurements of gas-phase organic compounds in the atmosphere during the New England Air Quality Study (NEAQS) in 2002, J. Geophys. Res., 108(D21), 4682, doi:10.1029/2003JD003863, 2003.

Hallquist, M., Wenger, J. C., Baltensperger, U., Rudich, Y., Simpson, D., Claeys, M., Dommen, J., Donahue, N. M., George, C., Goldstein, a. H., Hamilton, J. F., Herrmann, H., Hoffmann, T., Iinuma, Y., Jang, M., Jenkin, M., Jimenez, J. L., Kiendler-Scharr, a., Maenhaut, W., McFiggans, G., Mentel, T. F., Monod, a., Prévôt, a. S. H., Seinfeld, J. H., Surratt, J. D., Szmigielski, R. and Wildt, J.: The formation, properties and impact of secondary organic aerosol: current and emerging issues, Atmos. Chem. Phys., 9, 5155-5236, doi:10.5194/acp-9-5155-2009, 2009.

Heald, C. L., Jacob, D. J., Park, R. J., Russell, L. M., Huebert, B. J., Seinfeld, J. H., Liao, H. and Weber, R. J.: A large organic aerosol source in the free troposphere missing from current models, Geophys. Res. Lett., 32(L18809), doi:10.1029/2005GL023831, 2005.

Hildebrandt, L., Donahue, N. M. and Pandis, S. N.: High formation of secondary organic aerosol from the photo-oxidation of toluene, Atmos. Chem. Phys., 9, 2973–2986, doi:10.5194/acp-9-2973-2009, 2009.

Hildebrandt, L., Henry, K., Kroll, J. H., Pandis, S. N. and Donahue, N. M.: Evaluating the Mixing of Organic Aerosol Components using High-Resolution Aerosol Mass Spectrometry, Environ. Sci. Technol., 45, 6329–6335, doi:10.1021/es200825g, 2011.

Hildebrandt, L., Kostenidou, E., Mihalopoulos, N., Worsnop, D. R., Donahue, N. M. and Pandis, S. N.: Formation of highly oxygenated organic aerosol in the atmosphere: Insights from the Finokalia Aerosol Measurement Experiments, Geophys. Res. Lett., 37 (L23801), doi:10.1029/2010GL045193, 2010.

Jimenez, J. L., Canagaratna, M. R., Donahue, N. M., Prevot, a S. H., Zhang, Q., Kroll, J. H., DeCarlo, P. F., Allan, J. D., Coe, H., Ng, N. L., Aiken, a C., Docherty, K. S., Ulbrich, I. M., Grieshop, a P., Robinson, a L., Duplissy, J., Smith, J. D., Wilson, K. R., Lanz, V. a, Hueglin, C.,

1 Sun, Y. L., Tian, J., Laaksonen, a, Raatikainen, T., Rautiainen, J., Vaattovaara, P., Ehn, M.,

2 Kulmala, M., Tomlinson, J. M., Collins, D. R., Cubison, M. J., Dunlea, E. J., Huffman, J. a,

3 Onasch, T. B., Alfarra, M. R., Williams, P. I., Bower, K., Kondo, Y., Schneider, J., Drewnick, F.,

4 Borrmann, S., Weimer, S., Demerjian, K., Salcedo, D., Cottrell, L., Griffin, R., Takami, a,

5 Miyoshi, T., Hatakeyama, S., Shimono, a, Sun, J. Y., Zhang, Y. M., Dzepina, K., Kimmel, J. R.,

6 Sueper, D., Jayne, J. T., Herndon, S. C., Trimborn, a M., Williams, L. R., Wood, E. C.,

7 Middlebrook, a M., Kolb, C. E., Baltensperger, U. and Worsnop, D. R.: Evolution of organic

8 aerosols in the atmosphere., Science, 326(5959), 1525–9, doi:10.1126/science.1180353, 2009.

9 Kanakidou, M., Seinfeld, J. H., Pandis, S. N., Barnes, I., Dentener, F. J., Facchini, M. C., Van

10 Dingenen, R., Ervens, B., Nenes, A., Nielsen, C. J., Swietlicki, E., Putaud, J. P., Balkanski, Y.,

11 Fuzzi, S., Horth, J., Moortgat, G. K., Winterhalter, R., Myhre, C. E. L., Tsigaridis, K., Vignati,

12 E., Stephanou, E. G. and Wilson, J.: Organic aerosol and global climate modelling: a review,

13 Atmos. Chem. Phys., 5, 1053–1123, doi:10.5194/acp-5-1053-2005, 2005.

14 Kostenidou, E., Pathak, R. K. and Pandis, S. N.: An Algorithm for the Calculation of Secondary

15 Organic Aerosol Density Combining AMS and SMPS Data, Aerosol Sci. Technol., 41(11),

16 1002–1010, doi:10.1080/02786820701666270, 2007.

17 Kroll, J. H., Chan, A. W. H., Ng, N. L., Flagan, R. C. and Seinfeld, J. H.: Reactions of

18 Semivolatile Organics and their effects on Secondary Organic Aerosol Formation, Environ. Sci.

19 Technol., 41, 3545–3550, doi:10.1021/es062059x, 2007.

20 Kroll, J. H., Donahue, N. M., Jimenez, J. L., Kessler, S. H., Canagaratna, M. R., Wilson, K. R.,

21 Altieri, K. E., Mazzoleni, L. R., Wozniak, A. S., Bluhm, H., Mysak, E. R., Smith, J. D., Kolb, C.

22 E. and Worsnop, D. R.: Carbon oxidation state as a metric for describing the chemistry of

23 atmospheric organic aerosol., Nat. Chem., 3(2), 133–9, doi:10.1038/nchem.948, 2011.

24 Kroll, J. H. and Seinfeld, J. H.: Chemistry of secondary organic aerosol: Formation and evolution

25 of low-volatility organics in the atmosphere, Atmos. Environ., 42(16), 3593–3624,

26 doi:10.1016/j.atmosenv.2008.01.003, 2008.

Kroll, J. H., Smith, J. D., Che, D. L., Kessler, S. H., Worsnop, D. R. and Wilson, K. R.: Measurement of fragmentation and functionalization pathways in the heterogeneous oxidation of oxidized organic aerosol, Phys. Chem. Chem. Phys., 11(Physical Chemistry of Aerosols), 8005–8014, 2009.

Lathem, T. L., Beyersdorf, A. J., Thornhill, K. L., Winstead, E. L., Cubison, M. J., Hecobian, A. H., Jimenez, J. L., Weber, R. J., Anderson, B. E. and Nenes, A.: Analysis of CCN activity of Arctic aerosol and Canadian biomass burning during summer, Atmos. Chem. Phys., 13, 2735–2756, doi:10.5194/acp-13-2735-2013, 2013.

Lee, B. H., Kostenidou, E., Hildebrandt, L., Riipinen, I., Engelhart, G. J., Mohr, C., DeCarlo, P. F., Mihalopoulos, N., Prevot, a. S. H., Baltensperger, U. and Pandis, S. N.: Measurement of the ambient organic aerosol volatility distribution: application during the Finokalia Aerosol Measurement Experiment (FAME-2008), Atmos. Chem. Phys., 10(24), 12149–12160, doi:10.5194/acp-10-12149-2010, 2010.

Lee, B.-H. and Pandis, S. N.: Volatility of atmospheric organic aerosol, Carnegie Mellon University, Pittsburgh., 2010.

Massoli, P., Lambe, a. T., Ahern, a. T., Williams, L. R., Ehn, M., Mikkilä, J., Canagaratna, M. R., Brune, W. H., Onasch, T. B., Jayne, J. T., Petäjä, T., Kulmala, M., Laaksonen, a., Kolb, C. E., Davidovits, P. and Worsnop, D. R.: Relationship between aerosol oxidation level and hygroscopic properties of laboratory generated secondary organic aerosol (SOA) particles, Geophys. Res. Lett., 37(24), doi:10.1029/2010GL045258, 2010.

Matsunaga, A. and Ziemann, P. J.: Gas-Wall Partitioning of Organic Compounds in a Teflon Film Chamber and Potential Effects on Reaction Product and Aerosol Yield Measurements, Aerosol Sci. Technol., 44, 881–892, doi:10.1080/02786826.2010.501044, 2010.

Meyer, N. K., Duplissy, J., Gysel, M., Metzger, A., Dommen, J., Weingartner, E., Alfarra, M. R., Fletcher, C., Good, N., McFiggans, G., Jonsson, Å. M., Hallquist, M., Baltensperger, U. and Ristovski, Z. D.: Analysis of the hygroscopic and volatile properties of ammonium sulphate

seeded and un-seeded SOA particles, Atmos. Chem. Phys., 9, 721–732, doi:10.5194/acpd-8-8629-2008, 2009.

Moore, R. H., Nenes, A. and Medina, J.: Scanning Mobility CCN Analysis—A Method for Fast Measurements of Size-Resolved CCN Distributions and Activation Kinetics, Aerosol Sci. Technol., 44(10), 861–871, doi:10.1080/02786826.2010.498715, 2010.

Pandis, S. N., Harley, R. A., Cass, G. R. and Seinfeld, J. H.: Secondary Organic Aerosol Formation And Transport, Atmos. Environ. Part A-General Top., 26 13), 2269–2282, doi:10.1016/0960-1686(92)90358-R, 1992.

Petters, M. D. and Kreidenweis, S. M.: A single parameter representation of hygroscopic growth and cloud condensation nucleus activity, Atmos. Chem. Phys., 7(8), 1961–1971, doi:10.5194/acp-7-1961-2007, 2007.

Poulain, L., Wu, Z., Petters, M. D., Wex, H., Hallbauer, E., Wehner, B., Massling, A., Kreidenweis, S. M. and Stratmann, F.: Towards closing the gap between hygroscopic growth and CCN activation for secondary organic aerosols – Part 3: Influence of the chemical composition on the hygroscopic properties and volatile fractions of aerosols, Atmos. Chem. Phys., 10, 3775–3785, doi:10.5194/acpd-9-16683-2009, 2010.

Riipinen, I., Pierce, J. R., Donahue, N. M. and Pandis, S. N.: Equilibration time scales of organic aerosol inside thermodenuders: Evaporation kinetics versus thermodynamics, Atmos. Environ., 44, 597–607, doi:10.1016/j.atmosenv.2009.11.022, 2010.

Sareen, N., Schwier, A. N., Lathem, T. L., Nenes, A. and McNeill, V. F.: Surfactants from the gas phase may promote cloud droplet formation., Proc. Natl. Acad. Sci. U. S. A., 110(8), 2723–8, doi:10.1073/pnas.1204838110, 2013.

Shrivastava, M. K., Zelenyuk, A., Imre, D., Easter, R. C., Beranek, J., Zaveri, R. A. and Fast, J. D.: Implications of low volatility SOA and gas-phase fragmentation reactions on SOA loadings and their spatial and temporal evolution in the atmosphere, J. Geophys. Res. Atmos., 118(8), 3328–3342, doi:10.1002/jgrd.50160, 2013.

1 Surratt, J. D., Murphy, S. M., Kroll, J. H., Ng, N. L., Hildebrandt, L., Sorooshian, A.,

2 Szmigielski, R., Vermeylen, R., Maenhaut, W., Claeys, M., Flagan, R. C. and Seinfeld, J. H.:

3 Chemical Composition of Secondary Organic Aerosol Formed from the Photooxidation of

4 Isoprene, J. Phys. Chem. A, 110, 9665–9690, 2006.

5 Tritscher, T., Dommen, J., DeCarlo, P. F., Gysel, M., Barmet, P. B., Praplan, a. P., Weingartner,

6 E., Prévôt, a. S. H., Riipinen, I., Donahue, N. M. and Baltensperger, U.: Volatility and

7 hygroscopicity of aging secondary organic aerosol in a smog chamber, Atmos. Chem. Phys.,

8 11(22), 11477–11496, doi:10.5194/acp-11-11477-2011, 2011.

9 Volkamer, R., Jimenez, J. L., San Martini, F., Dzepina, K., Zhang, Q., Salcedo, D., Molina, L.

10 T., Worsnop, D. R. and Molina, M. J.: Secondary organic aerosol formation from anthropogenic

11 air pollution: Rapid and higher than expected, Geophys. Res. Lett., 33,

12 doi:10.1029/2006GL026899, 2006.

13 Vutukuru, S., Griffin, R. J. and Dabdub, D.: Simulation and analysis of secondary organic

14 aerosol dynamics in the South Coast Air Basin of California, J. Geophys. Res., 111(D10),

15 doi:D10s12 Artn d10s12, 2006.

16 Zhang, Q., Jimenez, J. L., Canagaratna, M. R., Allan, J. D., Coe, H., Ulbrich, I., Alfarra, M. R.,

17 Takami, A., Middlebrook, A. M., Sun, Y. L., Dzepina, K., Dunlea, E., Docherty, K., DeCarlo, P.

18 F., Salcedo, D., Onasch, T., Jayne, J. T., Miyoshi, T., Shimono, A., Hatakeyama, S., Takegawa,

19 N., Kondo, Y., Schneider, J., Drewnick, F., Borrmann, S., Weimer, S., Demerjian, K., Williams,

20 P., Bower, K., Bahreini, R., Cottrell, L., Griffin, R. J., Rautiainen, J., Sun, J. Y., Zhang, Y. M.

21 and Worsnop, D. R.: Ubiquity and dominance of oxygenated species in organic aerosols in

22 anthropogenically-influenced Northern Hemisphere midlatitudes, Geophys. Res. Lett., 34(13),

23 L13801, doi:10.1029/2007gl029979, 2007.

24

Table 1. Experimental Conditions

Expt. #	Seeds [a]	$[\text{Toluene}]_0$ [b] (ppb)	$[\text{Toluene}]_f$ [c] (ppb)	HONO injections	Lights (%)	[OH] exposure [d] (cm^{-3} s)
1	Yes	~ 300	na	1	33	na
2	No	~ 200	na	1+1	100	na
3	Yes	~ 300	na	1+1	100	na
4	No	~ 200	na	2	100	na
5	Yes	~ 100	na	2+1	100	na
6	No	~ 100 [e]	na	2	100	na
7	Yes	1320	1130	1	33	3.1×10^{10}
8	Yes	91 [g]	51 [h]	1	100	10×10^{10}
9	Yes	115	28	3+3	100	24×10^{10}

[a] $(NH_4)_2SO_4$ seed particles were used in some experiments

[b] Initial toluene concentrations estimated based on volume of VOC injected for Expts. 1-6 and measured by PTR-MS for Expts. 7-9

[c] Final toluene concentration after OH exposure

[d] Total OH exposure over the course of the experiment, estimated from exponential fits to the decay of toluene. Data not available for experiments 1-6 due to lack of PTR-MS data.

[e] Also injected 5 μl of benzene, o-xylene and 1,2,4-trimethylbenzene

[g] Also injected 16 ppb ethylbenzene, 12 ppb benzene and 23 ppb 1,2,4-trimethylbenzene

[h] Final concentrations of ethylbenzene, benzene and 1,2,4-trimethylbenzene: 9 ppb, 7 ppb and 13 ppb, respectively

1 Table 2. Summary of organic aerosol composition and volatility

Expt #	$(NO+NO_2)/$ OA^a	OS_c [b]	O:C	$NO^+/$ NO_2^{+} [c]	$H_2O/$ $(CO_2+^{13}CO_2)$	$^{13}CO/$ $^{13}CO_2$ [c]	Volatility Reduction (25s) [e]	Volatility Reduction (15s) [e]
1	0.10	- 0.14	0.84	8.2	1.70	1.17	3.5	3.6
2	0.11	0.16	0.83	7.5	0.30	1.09	30.4	30.8
3	0.10	0.00	1.04	8.3	2.35	1.23	3.1	3.6
4	0.12	0.01	0.92	7.9	1.70	1.22	3.5	4.0
5	0.12	- 0.14	0.94	8.0	2.10	1.22	1.9	2.2
6	0.10	- 0.17	0.89	8.6	1.99	1.36	1.7	2.5
7	0.13	- 0.29	0.76	8.2	1.85	n/a[d]	1.0	1.0
8	0.10	- 0.05	0.94	7.3	1.67	1.13	4.3	4.9
9	0.12	- 0.04	1.02	7.0	2.40	1.13	6.2	8.2

2
3 [a] After first period of lights on. OA includes NO^+ and NO_2^+.

4 [b] After first period of lights on, OS_c approximated as $2 \times O:C$ - H:C.

5 [c] From linear regressions throughout the experiment (when OA present).

6 [d] Not applicable (no isotopically labeled VOC used in experiment 7)

7 [e] Volatility reduction estimated for data collected at residence times of 15 s and 25 s. Values are calculated relative
8 to experiment 7 which featured the highest volatility.

1

2
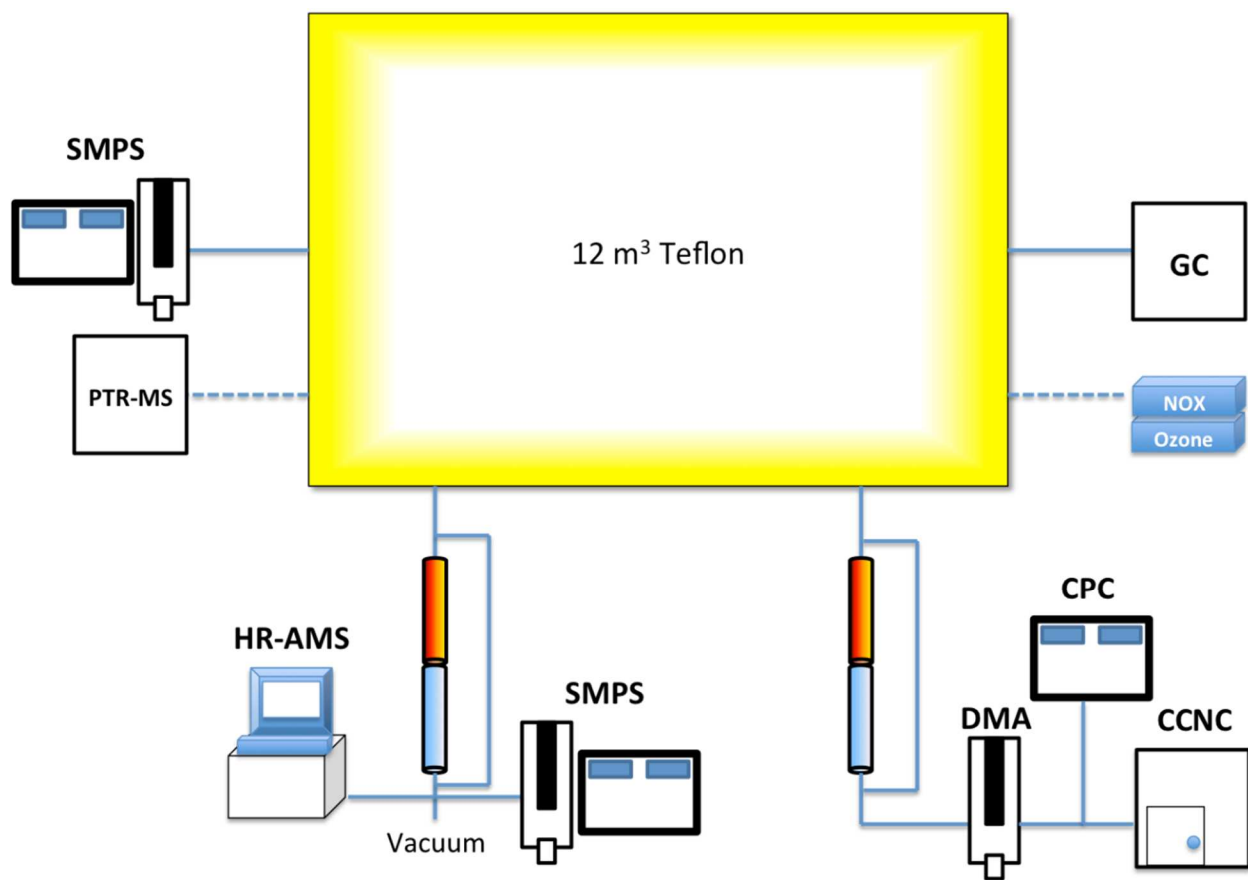
Figure 1. Schematic of experimental set-up. Dotted lines indicate that the equipment was used in
selected experiments.

5

Experiment 2
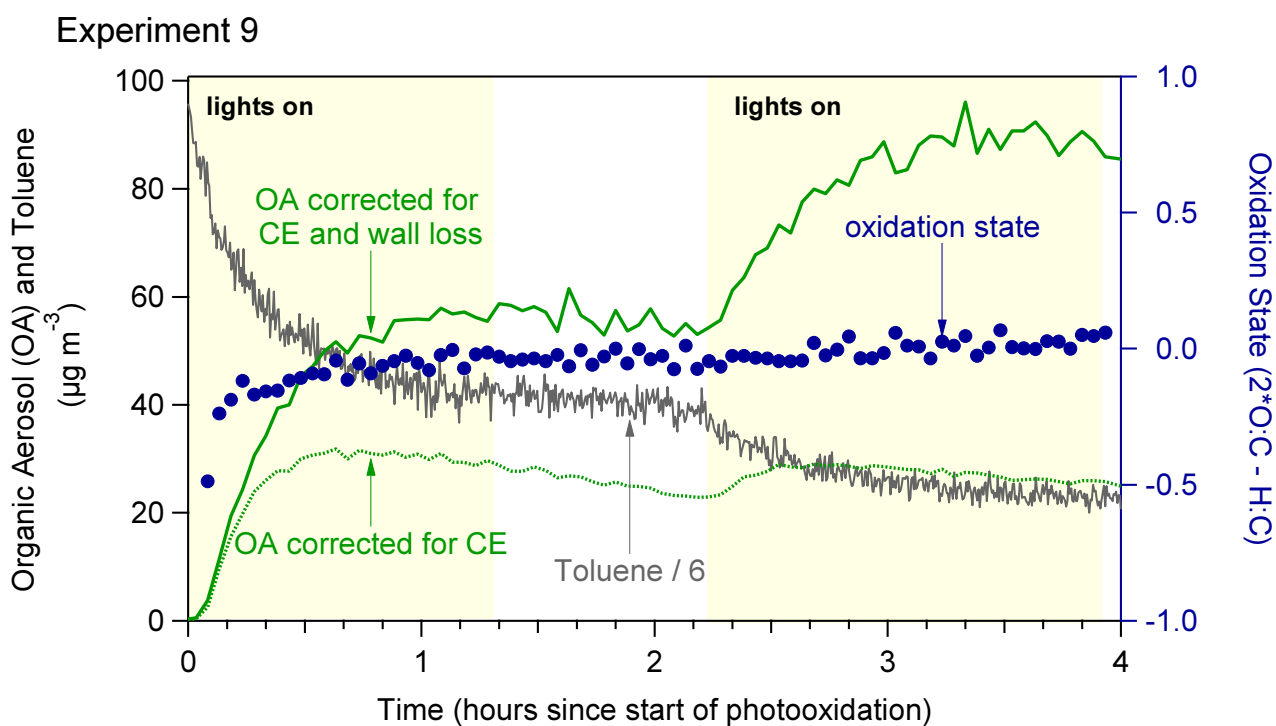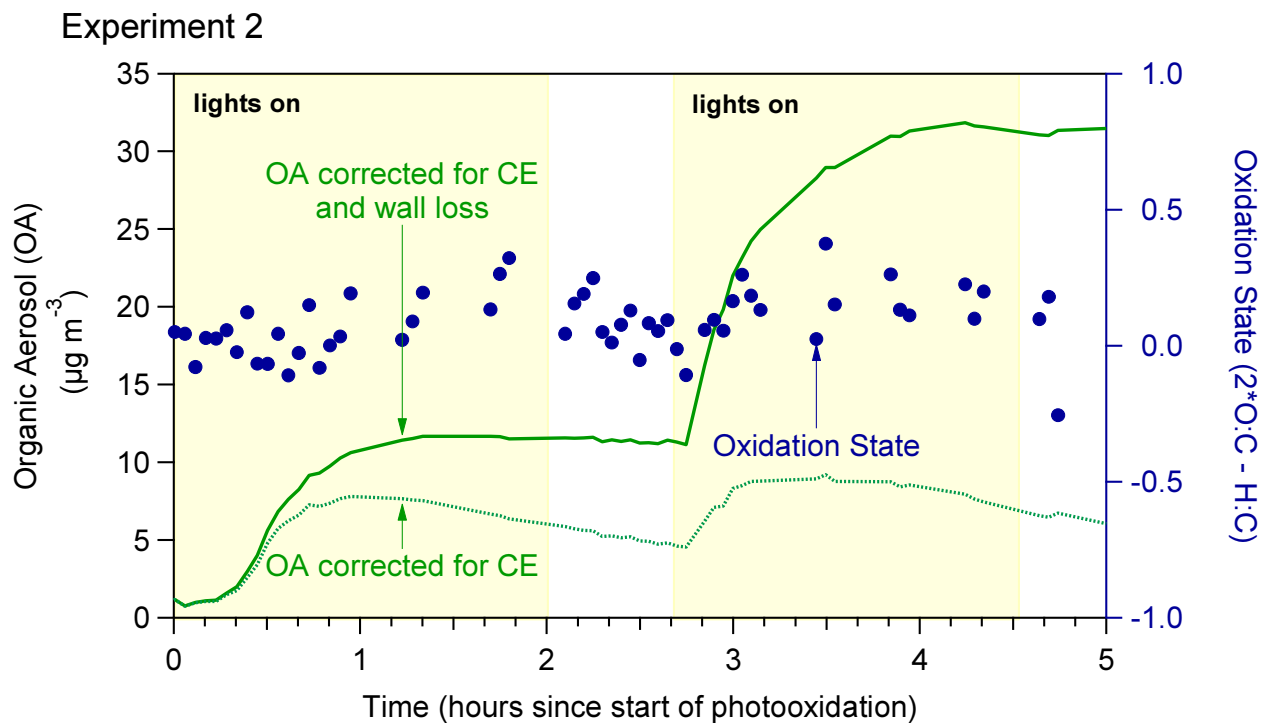
Experiment 9

Figure 2. Time series of OA concentration (corrected for CE and corrected for CE and wall loss) from an unseeded experiment (2, top) and a seeded experiment (9, bottom), both with two photo-oxidation periods ("lights on") before which HONO was injected. The periods during which the

1 reactor was dark are shown with white background while the periods with UV-lights are shaded

2 yellow. Also shown is the OA oxidation state (right axis) and concentrations of toluene during

3 Expt. 9 (toluene concentrations have been divided by 6 on the figure for easier readability).

4

5

6

7
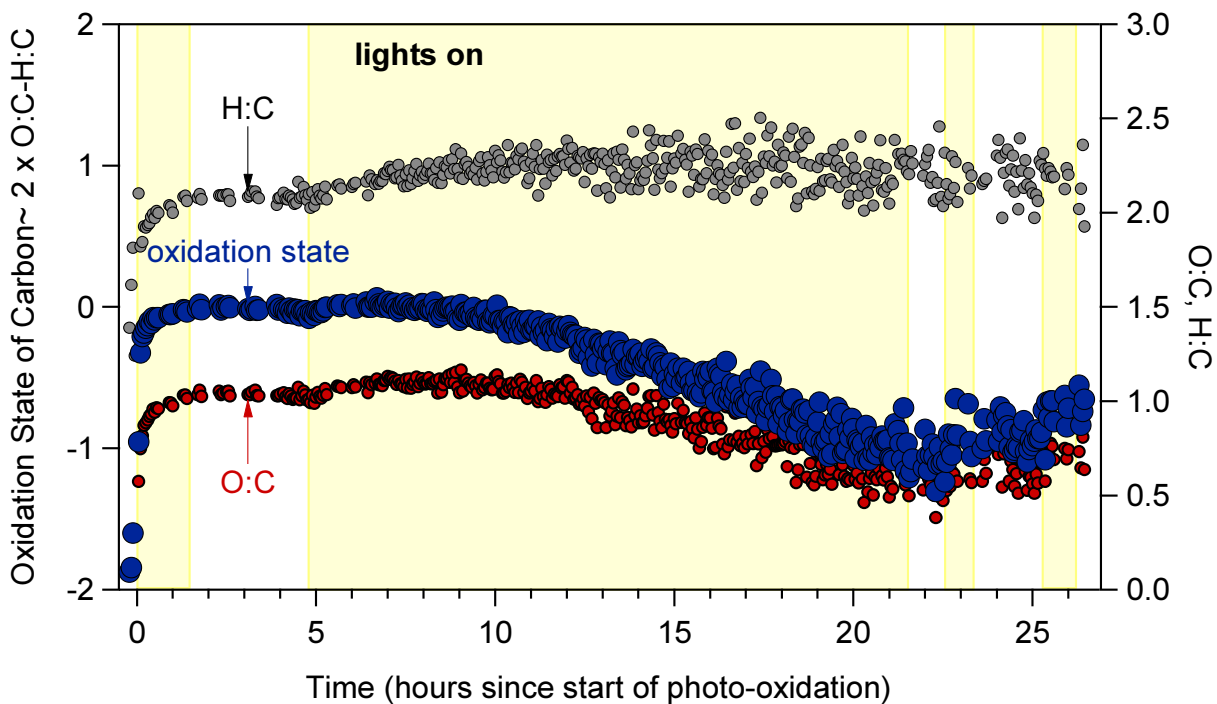
Figure 3. Time series of carbon oxidation state (left axis) and elemental ratios of O:C and H:C

(right axis) for Expt. 3. The periods during which the reactor was dark are shown in with white

background while the periods with UV-lights are shaded yellow.
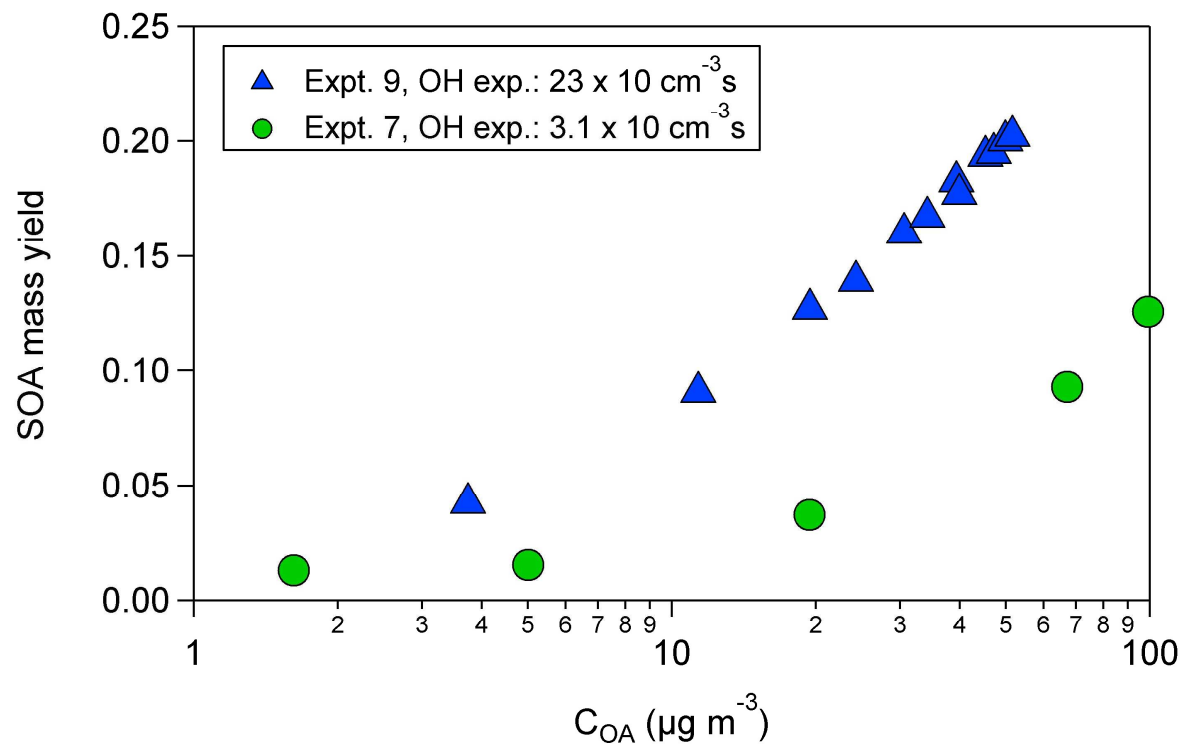
Figure 4. Organic aerosol mass yields for Expts. 7 and 9.
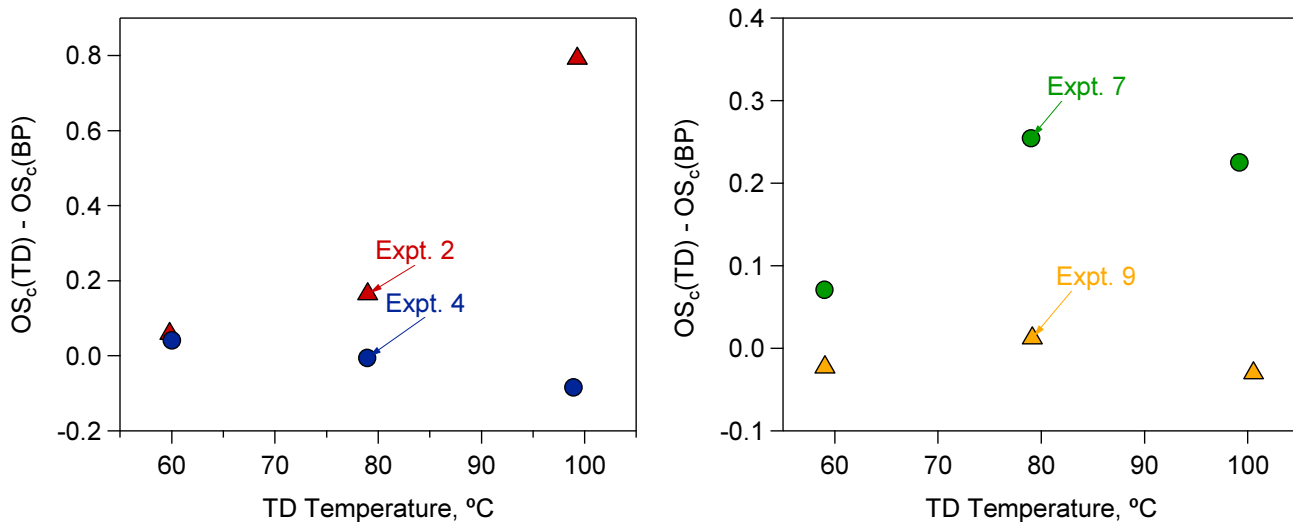
Figure 5. Comparison of the difference in oxidation state of denuded and total OA versus TD temperature for two unseeded experiments (2 and 4, left panel) and two seeded experiments (7 and 9, right panel). For OA of intermediate oxidation state (around 0, Expts. 4 and 9), oxidation state of the denuded OA is similar to the oxidation state of the full OA, implying that oxidation state does not correlate significantly with volatility. For OA of higher or lower oxidation state (Expts. 2 and 7, respectively) oxidation state anti-correlates with volatility, shown here as an increase in oxidation state difference with TD temperature.

1

2
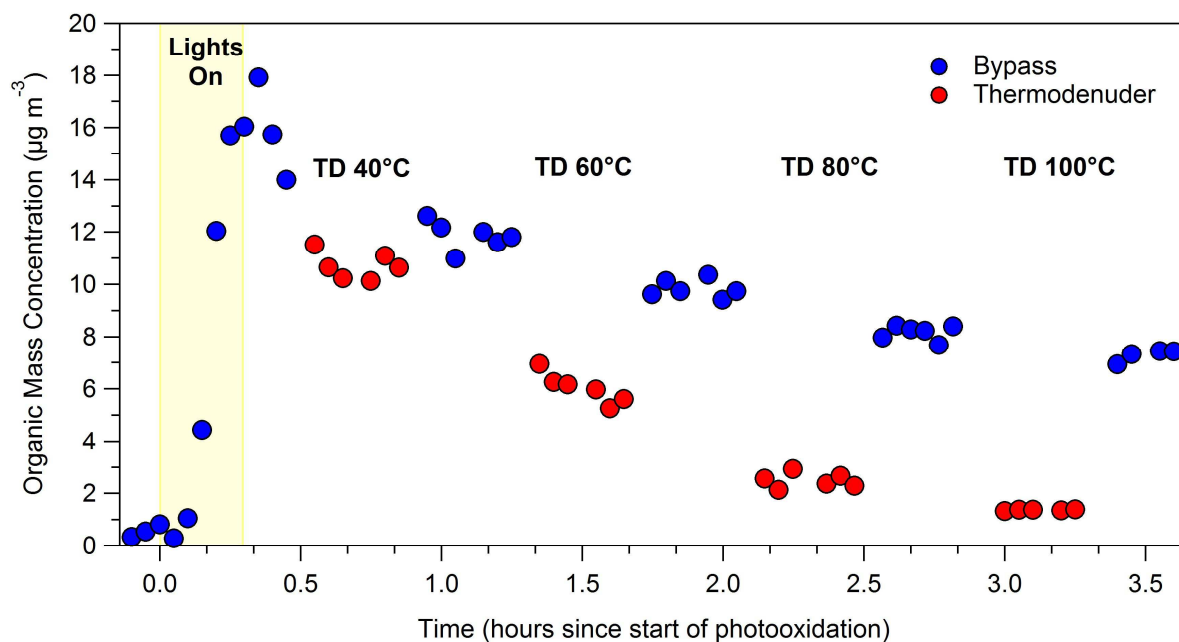
3   **Figure 6.** Bypass (blue) and thermodenuder (red) organic mass concentration time series for

4   Expt. 7. The yellow shaded region denotes time when the UV lights were on. Temperatures

5   represent the TD setpoint temperature. The bypass data have not been corrected for losses to the

6   walls of the chamber. The TD measurements have not been corrected for losses in the TD.
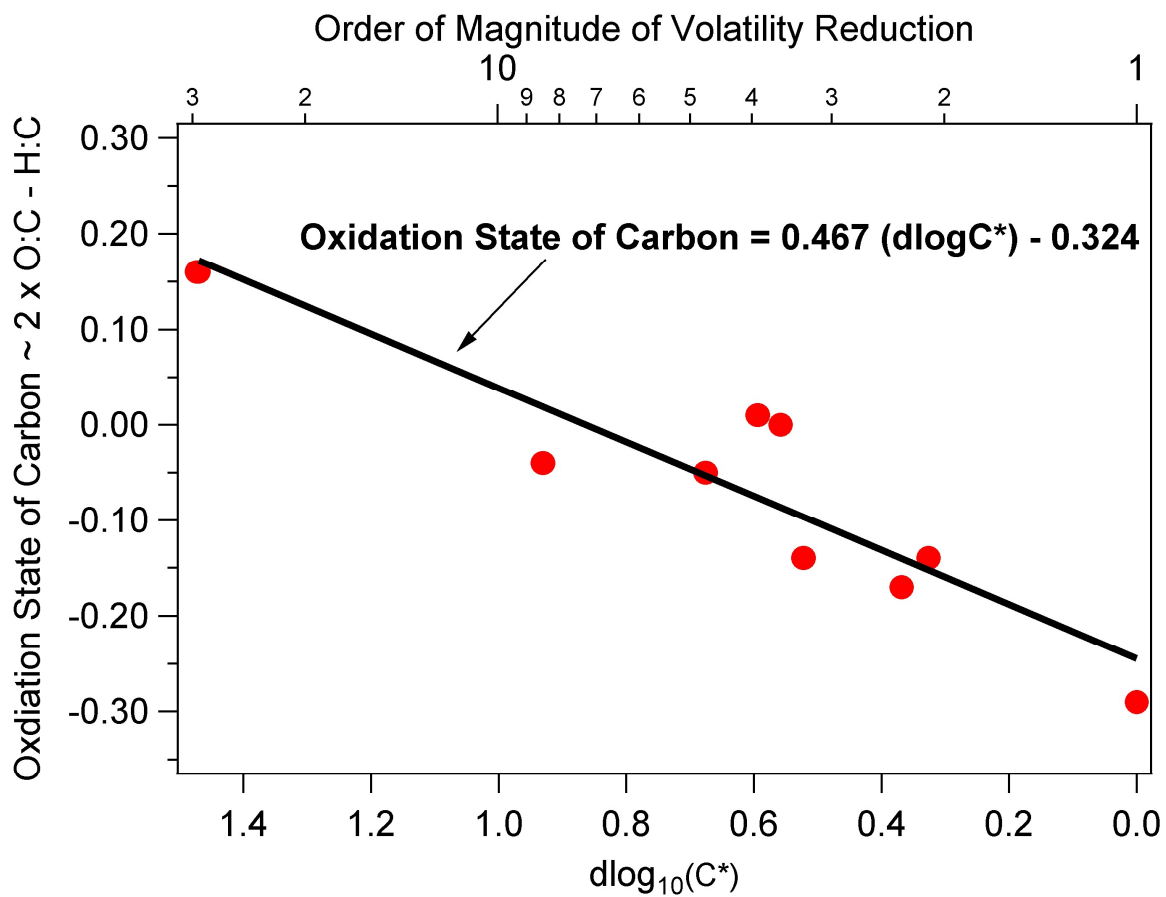
7

1
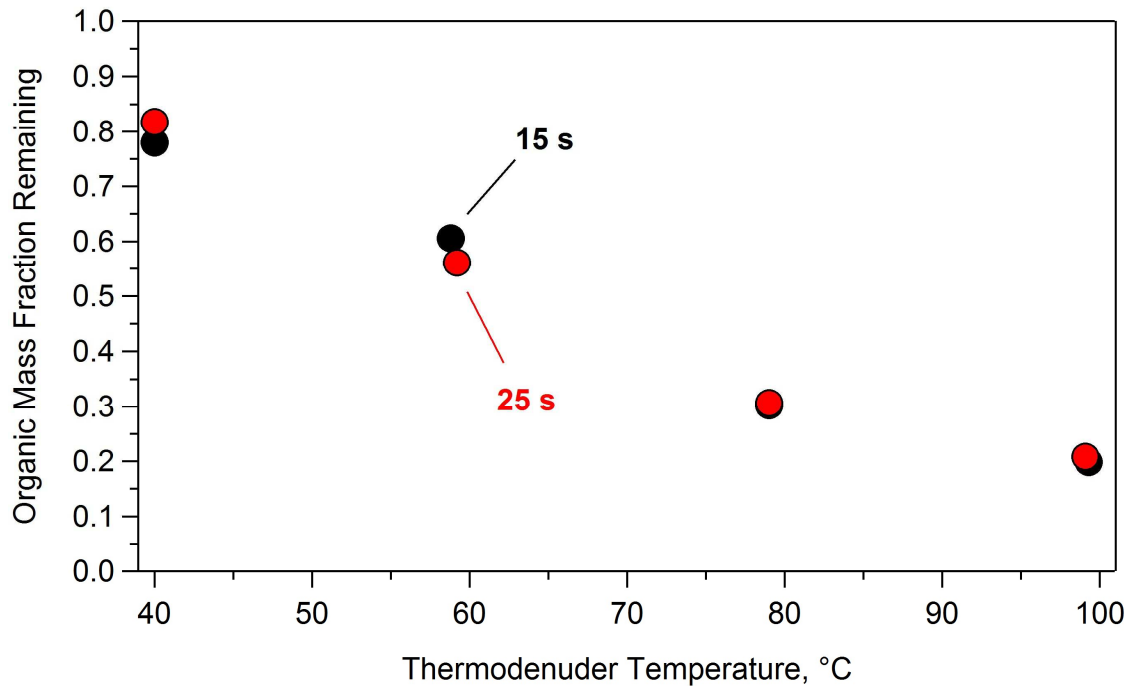
2

3

4   **Figure 7.** Organic mass fraction remaining as a function of thermodenuder temperature at a

5   residence time of 15 s (black) and 25 s (red) for Expt. 7. Thermograms have been corrected for

6   TD losses.
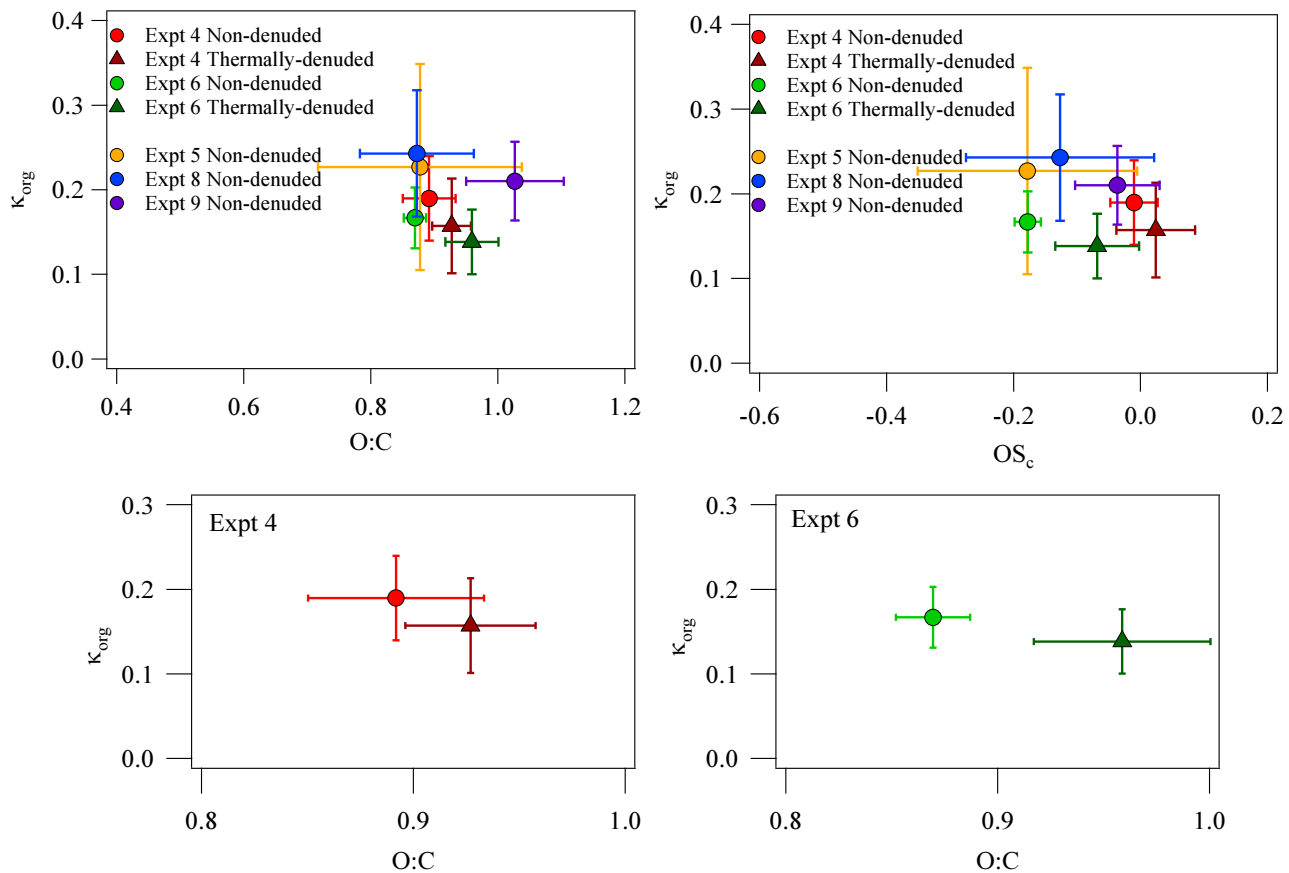
7

8

Figure 8. Oxidation state and volatility reduction in terms of change of log C* for the toluene SOA system. Red circles represent a single experiment and a single best-fit (black) line shows the trend.

1

Figure 9. κ_{org} versus O:C (top, left) and OS_c (top, right) for all experiments as listed in Table 1.

Also shown are magnified hygroscopicity and O:C for unseeded experiments with non-denuded

and thermally-denuded measurements (bottom). Vertical and horizontal error bars represent the

standard deviation in κ_{org} and O:C or OS_c, respectively.